RSC Advances

ROYAL SOCIETY OF CHEMISTRY

www.rsc.org/advances

One-pot synthesis of $Mn(MnO)/Mn_5C_2$/carbon nanotubes nanocomposite for supercapacitors

Jinhui Zhang[a,b], Jianbing Zang[a], Yanhui Wang*[a], Guoxiang Xin[a], Yan Zhang[a]

Received (in XXX, XXX) Xth XXXXXXXXX 20XX, Accepted Xth XXXXXXXXX 20XX
DOI: 10.1039/b000000x

We reported a one-pot synthesis of $Mn(MnO)/Mn_5C_2$/carbon nanotubes (CNTs) nanocomposite for supercapacitors. The $Mn(MnO)/Mn_5C_2$/CNTs composed of Mn(MnO) nanoflakes bonded with CNTs through interficial carbides Mn_5C_2 was prepared by heating a mixture of Mn powder and CNTs at 600 °C under vacuum. The carbides obtained by in-situ reaction provided a strong interface bonding between CNTs and Mn(MnO), and consequently enhanced stability of the nanocomposite as a supercapacitor electrode material. The capacitive properties of the $Mn(MnO)/Mn_5C_2$/CNTs electrodes were investigated by cyclic voltammetry (CV) test in 0.5 M Na_2SO_4 aqueous solution. The $Mn(MnO)/Mn_5C_2$/CNTs prepared at 600 °C for 1 h displayed maximum specific capacitance of 378.9 F g^{-1} (based on total mass of active materials) at 2 mV s^{-1}. Long-term cycling stability of the $Mn(MnO)/Mn_5C_2$/CNT electrode was investigated by repeating CV test from 0.1 and 0.8 V (vs. SCE) at 100 mV s^{-1}. Contrary to traditional MnO_2/CNTs electrode, whose specific capacitance would decrease with cycle number, the $Mn(MnO)/Mn_5C_2$/CNTs had an increased specific capacitance at the initial 450 cycles. This phenomenon is because of an electrochemical conversion from Mn(MnO) to MnO_2 in the initial CV test. Little decrease in specific capacitance was found even after 1000 cycles, indicating an excellent cycling stability. These properties are attributed to the unique $Mn(MnO)/Mn_5C_2$/CNT structure.

1. Introdution

Supercapacitors have become one of the most promising candidates for next-generation energy storage devices because of their high power density, fast charging−discharging rate, and excellent cycling stability.[1-4] Depending on charge-storage mechanism, supercapacitors are generally classified into electrical double-layer capacitors (EDLCs) and pseudo-capacitors (or redox supercapacitors).[5-8] For EDLCs, carbon-based materials with large surface area and high conductivity have been recognized as the most promising candidates.[9-13] However, carbon-based supercapacitors often suffer from a relatively low energy density limiting their real applications in energy storage systems. On the other hand, transition metal oxides and conducting polymers are considered to be typical active electrode materials for pseudo-capacitors, which utilize fast and reversible redox reactions at the surface of the electroactive material for charge storage.[14-16] Nevertheless, poor electrical conductivities of these materials and an irreversibility of Faradaic reaction on material surface usually cause a poor cycling stability. In recent years, MnO_2 as pseudocapacitive materials has attracted great interest because of its low cost, natural abundance, and environmental safety.[17, 18] However, the dense morphology of MnO_2 was unfavorable for the penetration of electrolyte into the bulk of the oxide materials, and its intrinsically poor electronic conductivity limited charge transfer reaction kinetics.[18-20] To solve these problems, various nanostructured MnO_2 have been successfully synthesized and characterized over the past few years. Nowdays, the researchers have been focused on improving the conductivity of MnO_2-based electrodes with the goal of maximizing its electrochemical utilization for charge storage. One effective approach is to synthesize composite nanostructures where thin MnO_2 layers are loaded on highly conductive materials such as conducting polymer,[21-23] carboneous materials,[24-27] metal.[28] In all of the above cases, MnO_2 coating on the surface of the substrate materials is synthesized in solution conditions. The contact resistance at the interface between MnO_2 coating and highly conductive substrate is often ignored.[18] Actually this contact resistance would reflect the conductive performance of the composite materials and limit fast electron transport from MnO_2 coating to substrate. Therefore, MnO_2-based composite material with a high electrical conductivity as well as more electron pathways for fast electron transport has become one focus in designing high-performance electrodes for supercapacitors.

Here, we designand synthesize a novel $Mn(MnO)/Mn_5C_2$/carbon nanotubes (CNTs) nanocomposite. The scheme of the deposition process is illustrated in Figure 1. The CNTs were uniformly mixed with metal Mn powder. When the mixture was heated in vacuum (10^{-1} Pa), the active metal Mn was volatilized at elevated temperature, and then deposited on the CNT surface, forming a Mn(MnO) layer. The even exposure of the CNTs to the volatilized Mn ensures a deposition layer on every nanotube, and also allows for mass production of deposited CNTs. The aims of designing such $Mn(MnO)/Mn_5C_2$/CNTs are considered as the following: (1) Mn, a strong carbide forming element, can consistently achieve low-resistance metal–tube ohmic contacts with CNTs, [29] which would be favor for a fast redox response. (2) The Mn(MnO) layer, can be electrochemically oxidized to MnO_2 layer in potential cycling process, providing a high pseudocapacitance.[30,31] Moreover, a strong bonding originated from the carbide layer would be favor to stabilize active material during the cycling process, resulting in a high cycling stability. So that the $Mn(MnO)/Mn_5C_2$/CNTs prepared at 600 °C for 1 h exhibited large specific capacitance of 378.9 F g^{-1} (based on total mass of active materials) at 2 mV s^{-1},

and excellent long-term cycling stability.

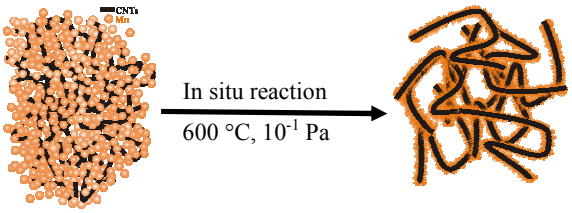

Fig. 1. Scheme of the deposition process.

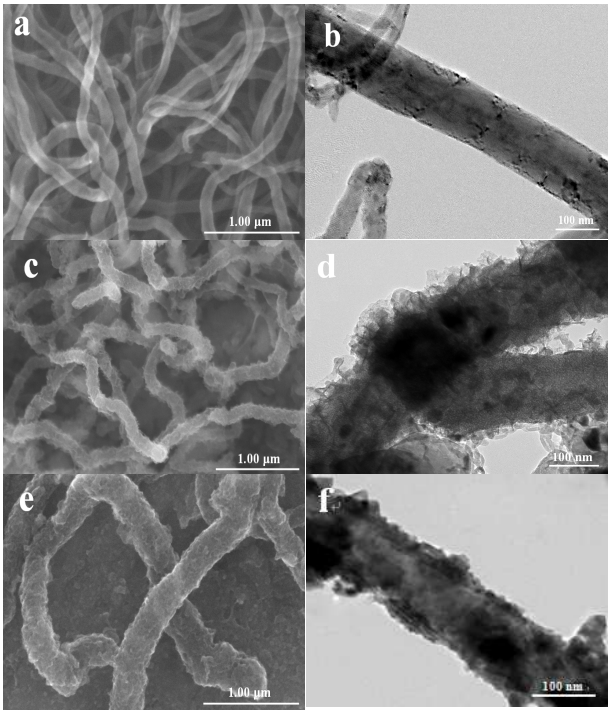

Fig. 2. FESEM and TEM images of pristine CNTs (a, b), Mn(MnO)/Mn_5C_2/CNTs-1 (c, d), and Mn(MnO)/Mn_5C_2/CNTs-2 (e, f).

2. Experimental

2.1 Preparation of Mn(MnO)/Mn_5C_2/CNTs

The CNTs prepared by CVD were purchased from Shenzhen Nanotech Port Limited Company. Their outer diameter and length were 80–100 nm and 5–15 μm, respectively. All the other chemicals in this paper were of analytical grade and were used without further purification. Mn(MnO)/Mn_5C_2/CNTs were fabricated via the following: (1) CNTs (0.5 g) without any pretreatment were sonicated in alcohol solution (100 mL) for two hours to form stable dispersions. Subsequently, the stable alcohol suspension was uniformly mixed with 10 g solid Mn powder (45 μm), when alcohol completely evaporating from mixture, placed them into small drum, then put them in a self-made vacuum reaction chamber. (2) The chamber was evacuated to a vacuum of 10^{-1} Pa, and then heated to the temperature of 600 °C for 1-2 h. Mn was evaporated and deposited on the CNT surface. After the deposition finished, shut off the heating switch, cool to room temperature. (3) We took the drum out. The resultant mixture contained both Mn(MnO)/Mn_5C_2/CNTs and remanent Mn powder. These were separated by ultrasonic treatment in acetone for 30 min, in which the Mn(MnO)/Mn_5C_2/CNTs readily formed a suspension. Finally, the suspension including Mn(MnO)/Mn_5C_2/CNTs was carefully removed and dried under vacuum at room temperature for 24 h. These samples prepared at 600 °C for 1-2 h were denoted as Mn(MnO)/Mn_5C_2/CNTs-1 and Mn(MnO)/Mn_5C_2/CNTs-2. The weight increments of the two samples were measured to be 200% and 300%, respectively.

2.2 Preparation of electrodes

The fabrication of working electrodes was carried out as described. The as-prepared nanocomposite (3 mg) with 15 wt.% carbon black and 5 wt.% polytetrafluoroethylene, and dispersed in ethanol to form slurry. Then the resulting mixture was coated onto the nickel foam substrate (0.5 cm×1 cm) with a spatula and pressed again, which was followed by drying at 100 °C for 12 h in a vacuum oven.

2.3 Material Characterization

The morphology of the Mn(MnO)/Mn_5C_2/CNTs was investigated with a JEM-2010 high-resolution transmission electron microscope (TEM) and field-emission scanning electron microscopy (FESEM; JEOL JEM-3000 equipped with energy dispersive spectroscopy (EDS), and the phase structure was identified by X-ray diffraction (XRD; Philips PW1730 diffractometer with Cu Ka radiation and a graphite monochrometer, k =1.54184).

2.4 Electrochemical measurement

Cyclic voltammetry (CV) and electrochemical impedance spectroscopy (EIS) were efficient techniques to evaluate active materials for supercapacitors. In this study, they were measured by a CHI 660C electrochemical workstation in a three electrode setup: A Ni foam coated with Mn(MnO)/Mn_5C_2/CNTs as the working electrode, a graphite sheet as the counter electrode, and a saturated calomel electrode (SCE) as the reference electrode. The measurements were carried out in a 0.5 M Na_2SO_4 aqueous solution at room temperature. CV tests were done between 0 and 0.8 V at different scan rates of 2, 10, 20, 50, and 100 mV s^{-1}, and EIS measurements were also carried out in the frequency range from 100 k to 0.01 Hz at open circuit potential with an ac perturbation of 5 mV. The specific capacitance of the electrode can be measured according to the following equation:

$$C = \frac{1}{v(Vc - Va)} \int_{Va}^{Vc} I(V)dV \quad (1)$$

Where C is the specific capacitance (F g^{-1}), v is the potential scan rate (mV s^{-1}), $Vc-Va$ is the sweep potential range during discharging (V) and $I(V)$ denotes the response current density (A g^{-1}).

3. Results and discussion

We prepared the Mn(MnO)/Mn_5C_2/CNT samples at 600 °C, 10^{-1} Pa for 1 and 2 h, respectively, and denoted as Mn(MnO)/Mn_5C_2/CNTs-1 and Mn(MnO)/Mn_5C_2/CNTs-2. Figure 2 shows the FESEM and TEM images of the pristine CNTs, Mn(MnO)/Mn_5C_2/CNTs-1 and Mn(MnO)/Mn_5C_2/CNTs-2. As shown in Figure 2a and b, the pristine multi-walled CNTs with diameters ranging from 80 to 100 nm are very clean and smooth.

Compared with the pristine CNTs, the morphology of the Mn(MnO)/Mn_5C_2/CNTs-1 shown in Figure 2c and d reveals that a thin layer of nanoflakes was formed on the surface of the CNTs, resulting in an increase in diameters. The thickness of the coating was about 40 nm. As deposition time prolonged, the coating became thicker and relatively denser, as shown in Figure 2e and f.

The phases of the as-prepared nanocomposites were determined by the XRD analysis. Figure 3 shows typical XRD patterns of the pristine CNTs, Mn(MnO)/Mn_5C_2/CNTs-1 and Mn(MnO)/Mn_5C_2/CNTs-2, respectively. A characteristic peak at around 26° (Figure 3a) is corresponding to the (002) plane of CNTs.[13] The others were attributed to Mn, MnO, and Mn_5C_2 phases. The active metal Mn, especially for nanoscale Mn film on CNTs, was easily oxidized even in the air. So the oxide MnO occurred in the coating. The presence of Mn_5C_2 indicated that the reaction occurred between CNTs and Mn(MnO) during deposition process. These results futher revealed that a typical interfacial diffusion reaction process that carbon atoms diffused from CNT to Mn(MnO) layer through the Mn_5C_2 layer occurred, and the diffused carbon atoms reacted with active metal Mn under high temperature. Therefore, Mn_5C_2 were infered to be located between Mn(MnO) and CNTs. As the deposition time prolonged, the relative intensity of C peaks decreased and the relative intensity of Mn_5C_2 peaks increased (as shown in Figure 3b), suggesting that more carbides were formed.

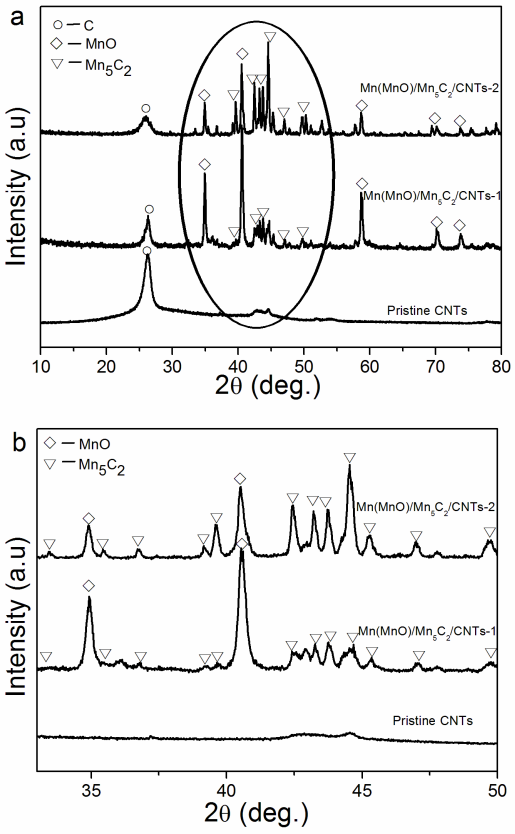

Fig. 3. (a) XRD patterns of pristine CNTs, Mn(MnO)/Mn_5C_2/CNTs-1, and Mn(MnO)/Mn_5C_2/CNTs-2. (b) Magnified regions from representative areas of the XRD patterns (33–50°) in (a).

The weight percentages of Mn_5C_2 and Mn(MnO) in the composites were estimated. After deposition, the weight increments of the samples can be attributed to the weights of the coating. Since the coatings can be dissolved in acid solution, we used hydrochloric acid to remove the coatings. The weight of the remained CNTs was smaller compared to the CNTs without coatings but underwent the same process. The weight decrease can be ascribed to formation of the carbides Mn_5C_2 followed by Equation 2. So the weight of the Mn_5C_2 can be calculated based on chemometrics, and the weight of Mn(MnO) was obtained by reducing the Mn_5C_2 weight from the coating weight. The results showed that the weight percentages of CNTs, Mn_5C_2 and Mn(MnO) in Mn(MnO)/Mn_5C_2/CNTs-1 were 32.3%, 13.5% and 54.2%, respectively. And for Mn(MnO)/Mn_5C_2/CNTs-2, they were 23.8%,16.8% and 59.4%, respectively.

$$5Mn+2C \rightarrow Mn_5C_2 \quad (2)$$

The morphologies of the CNTs obtained from acid-etched Mn(MnO)/Mn_5C_2/CNTs are shown in Figure 4. Compared to pristine CNTs (Figure 4a), the CNT walls became thinner and the surface turned rough after the coatings were removed (Figures 4b and c). This confirmed that the surface carbons reacted with the metal Mn and formed interfacial carbides during deposition. When the carbides were removed, the thickness of the CNTs reduced. Because more carbides formed in Mn(MnO)/Mn_5C_2/CNTs-2, the surfaces of the CNTs were rougher than those in eroded Mn(MnO)/Mn_5C_2/CNTs-1.

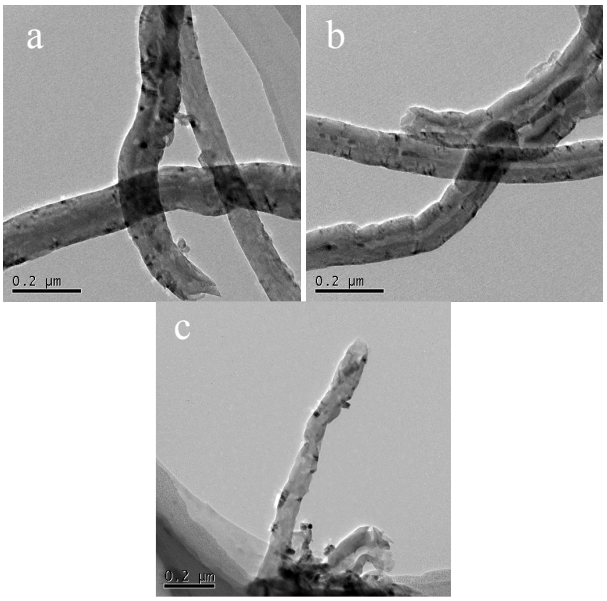

Fig. 4. TEM images of pristine CNTs (a), and CNTs obtained from Mn(MnO)/Mn_5C_2/CNTs-1 (b) and Mn(MnO)/Mn_5C_2/CNTs-2 (c) after the coatings were removed by acid-etching.

In order to evaluate the capacitive properties of the nanocomposite as supercapacitor electrode material, electrochemical measurements were conducted in a three-electrode electrochemical cell with a graphite sheet counter electrode and a saturated calomel reference electrode in 0.5 M Na_2SO_4 aqueous solution. Figure 5a shows the cyclic voltammetric (CV) curves of pristine CNT, Mn(MnO)/Mn_5C_2/CNTs-1, and Mn(MnO)/Mn_5C_2/CNTs-2 electrodes at 100 mV s^{-1}. The CV curve of pristine CNT electrode was close to rectangle, indicating an ideal electrical double-layer capacitance behavior.[32] In comparison to the CV curve of pristine CNT electrode, the Mn(MnO)/Mn_5C_2/CNTs-1, and Mn(MnO)/Mn_5C_2/CNTs-2 electrodes delivered an obviously higher current response, which can be attributed to

pseudocapacitive characteristic. It is also noted that the CV curves of the Mn(MnO)/Mn_5C_2/CNTs-1 electrode showed more quasi-rectangular shapes and higher current response compared with the Mn(MnO)/Mn_5C_2/CNTs-2 electrode, suggesting that the Mn(MnO)/Mn_5C_2/CNT-1 electrode possessed a more ideal capacitive behavior. Furthermore, Figure 5b and c show the effect of the scan rate on the CV response of the Mn(MnO)/Mn_5C_2/CNTs-1 and Mn(MnO)/Mn_5C_2/CNTs-2 electrodes. It is clearly observed that the shapes of these CV curves remained unchanged as the scan rate increase from 2 to 100 mV s^{-1}, indicating rapid current responses and low resistances of these nanocomposites.[19] The specific capacitance determined from the CV curves were calculated according to equation. Figure 5d shows specific capacitances of Mn(MnO)/Mn_5C_2/CNTs-1 and Mn(MnO)/Mn_5C_2/CNTs-2 electrodes at different scan rates. The Mn(MnO)/Mn_5C_2/CNTs-1 electrode showed larger specific capacitance, which was 378.9 F g^{-1} (based on total mass of active materials) at a scan rate of 2 mV s^{-1}, compared with the Mn(MnO)/Mn_5C_2/CNTs-2 electrode. The maximum energy density was 33.7 Wh/kg and the power density can reach to 6.1 kW/kg. The excellent electrochemical performances of the Mn(MnO)/Mn_5C_2/CNTs-1 electrode may be attributed to its unique structure: (1) A thin Mn(MnO) layer composed of nanoflakes on the surface of CNTs has a relatively porous architecture for the effective transport of electrolyte throughout the whole electrode, enabling a fast and reversible redox reaction; and (2) interficial carbide Mn_5C_2 is benefit for a low-resistance ohmic contact between MnO_2 layer and highly conductive CNT substrate, providing a shorter channel to CNTs for the electrons transport path. The decrease in specific capacitance of Mn(MnO)/Mn_5C_2/CNTs-2 electrode was attributed to relatively thicker coating and denser morphology.

The electrochemical performance of Mn(MnO)/Mn_5C_2/CNT electrode was further studied by electrochemical impedance spectroscopy (EIS) measurements. The Nyquist plots of the pristine CNTs, Mn(MnO)/Mn_5C_2/CNTs-1, and Mn(MnO)/Mn_5C_2/CNTs-2 electrodes are shown in Figure 6. The impedance spectra were all composed of a semicircular in high frequency region and a straight line in low frequency region. The intersection of the semicircular arc at real part Z' in high frequency range is the resistance (ESR), which represents the sum resistance of the electrochemical system.[29] From the inset of Figure 6, the ESRs of pristine CNTs, Mn(MnO)/Mn_5C_2/CNTs-1, and Mn(MnO)/Mn_5C_2/CNTs-2 electrodes were estimated to be 6.4, 5.3 and 8.2 Ω, respectively. The as-prepared electrodes had a lower series resistance compared to MnO_2/CNT composite reported in previous research whose series resistance were usually dozens of ohms.[33, 34] That was because the carbide formed a low-resistance ohmic contact between MnO_2 layer and CNTs, providing a direct path for the electron delivery from MnO_2 layer to CNTs. Moreover, the ESRs of Mn(MnO)/Mn_5C_2/CNTs-1 prepared high-temperature vacuum purification was lower than that of pristine CNTs, which was attributed to the lower contact barrier between them and nickel foam substrate. The vertical straight line in low frequency region revealed a pure capacitive behavior.[35] It was clearly seen that the Mn(MnO)/Mn_5C_2/CNTs-1 electrode had relatively ideal supercapacitor behave compared with Mn(MnO)/Mn_5C_2/CNTs-2 electrode, which corresponded to the CV results.

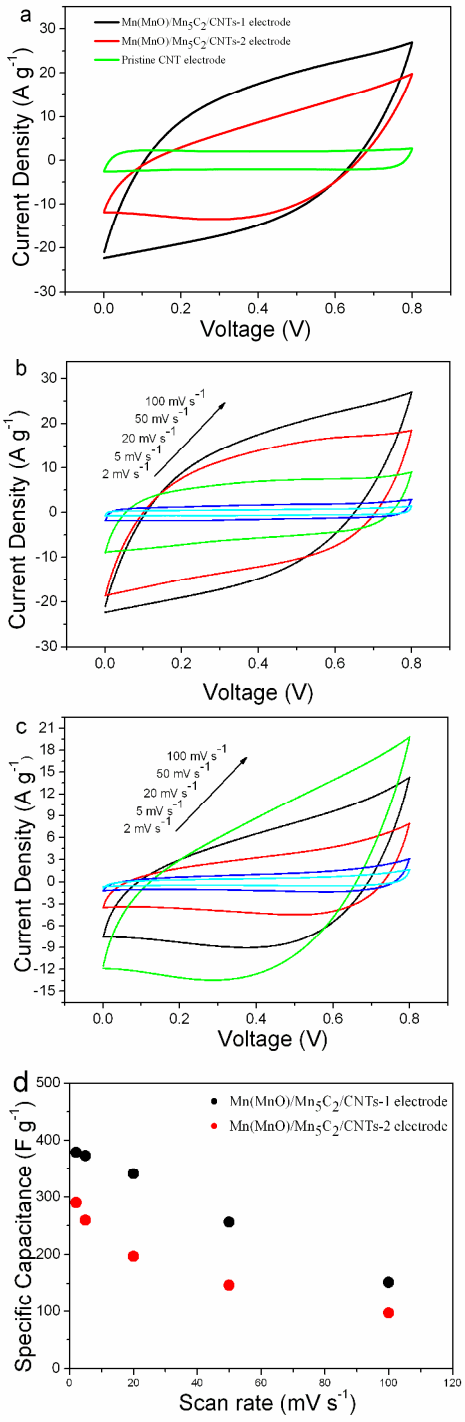

Fig. 5. (a) CV curves of pristine CNT, Mn(MnO)/Mn_5C_2/CNTs-1, and Mn(MnO)/Mn_5C_2/CNTs-2 electrodes in 0.5 M Na_2SO_4 aqueous solution at 100 mV s^{-1}, (b, c) CV curves of Mn(MnO)/Mn_5C_2/CNTs-1 and Mn(MnO)/Mn_5C_2/CNTs-2 electrodes at different scan rates in 0.5 M Na_2SO_4 aqueous solution. (d) Specific capacitances of Mn(MnO)/Mn_5C_2/CNTs-1 and Mn(MnO)/Mn_5C_2/CNT-2 electrodes at different scan rates derived from CV.

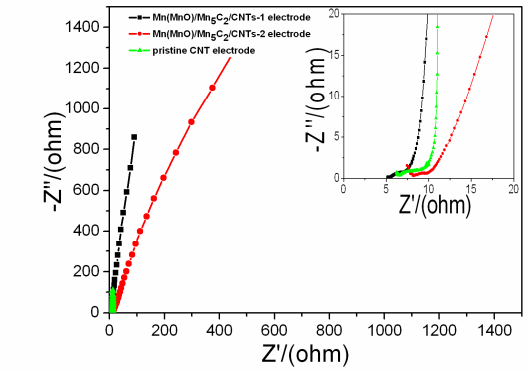

Fig. 6. Nyquist plots of pristine CNT, Mn(MnO)/Mn_5C_2/CNTs-1, and Mn(MnO)/Mn_5C_2/CNTs-2 electrodes. Inset is a magnified portion of the plot in the high frequency region.

The cycling stability of the nanocopmposites is an important performance for its practical applications. Herein, the cycling stability of the Mn(MnO)/Mn_5C_2/CNT electrodes were evaluated by repeating the CV test between 0.1 and 0.8 V (vs. SCE) at a scan rate of 100 mV s^{-1}. The capacitance retention ratio as a function of cycle number is presented in Figure 7. It can be noted that the specific capacitance increased with cycle numbers at the initial cycling (0-450 cycles). And then, it kept almost a constant until 1000 cycles, indicating an excellent cycling stability of the Mn(MnO)/Mn_5C_2/CNTs. Based on the above results, it can be inferred that the as-prepared nanocomposite used as an electrode material was activated by potential cycling at the initial stage. During potential cycling in aqueous Na_2SO_4 electrolyte, the outer (Mn)MnO layer was electrochemically oxidized to Mn_3O_4 and then to MnO_2. The reactions for the conversion of Mn(MnO) to MnO_2 was postulated as follows:[30, 31]

$$Mn\cdot 2H_2O + 2H_2O \rightarrow Mn(OH)_2 + 2H_3O^+ \quad (3)$$

$$MnO + H_2O \rightarrow Mn(OH)_2 \quad (4)$$

$$3Mn(OH)_2 \rightarrow Mn_3O_4\cdot 2H_2O + 2H^+ + 2e^- \quad (5)$$

$$2(Mn_3O_4\cdot 2H_2O) + 5OH^- \rightarrow 6MnO_2\cdot 5H_2O + 3H^+ + 8e^- \quad (6)$$

In order to prove the assumptions, the XRD pattern of the Mn(MnO)/Mn_5C_2/CNTs-1 after potential cycling for 300 cycles is given in Figure 8. In Figure 8a, except the peaks of MnO and Mn_5C_2, some peaks attributed to MnO_2 and Mn_3O_4 were also found. In order to futher prove this phenomenon, we have been showed the HRTEM image of Mn(MnO)/Mn_5C_2/CNTs-1 after 300 cycles (Fig. 8b). The lattice fringes of 0.49 nm corresponded to the (101) planes of Mn_3O_4, confirming the transformation of Mn(MnO) to MnO_2/Mn_3O_4. The conversions of Mn(MnO) to MnO_2 caused an increase in specific capacitance at first hundreds cycles. Once the conversions finished, the specific capacitance no longer increased, but it had almost no decrease even after 1000 cycles.

As we all know, MnO_2/carboneous composite electrodes often suffered the cycle degradation issues caused by mechanical problems, that is, the structure or volume changes during redox reactions leading to MnO_2 loss and film detachment from electrode surfaces. Compared to conventional composite electrode material, the unique structure of Mn(MnO)/Mn_5C_2/CNTs, in which the interficial carbide Mn_5C_2 formed a chemically strong bonding between CNTs and Mn(MnO), is great benefit to maintain the whole structural integrity of the nanocomposite. And therefore, the Mn(MnO)/Mn_5C_2/CNT electrode exhibited excellent cycling stability.

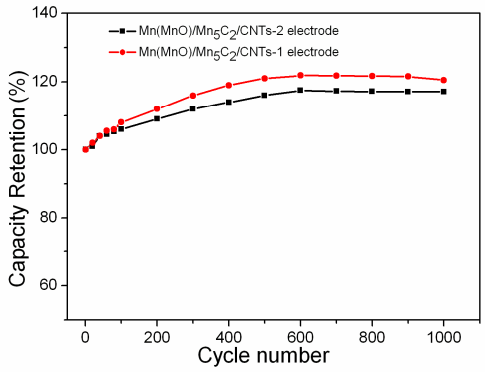

Fig. 7. Capacity retention from Mn(MnO)/Mn_5C_2/CNTs-1 and Mn(MnO)/Mn_5C_2/CNTs-2 electrodes as a function of number.

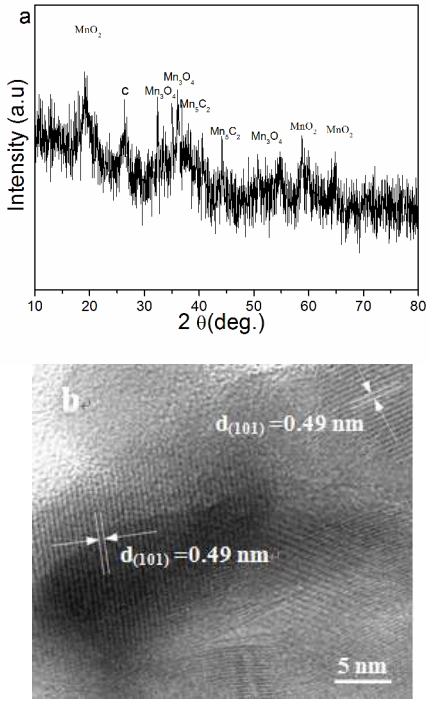

Fig. 8.(a) XRD pattern of Mn(MnO)/Mn_5C_2/CNTs-1 by repeating the CV test at 100 mV s^{-1} after 300 cycles.(b)HRTEM image of Mn(MnO)/Mn_5C_2/CNTs-1 after 300 cycles.

4. Conclusions

In summary, we successfully prepared a novel Mn(MnO)/Mn_5C_2/CNTs by one-pot heating a mixture of Mn powder and CNTs under vacuum. The thin Mn(MnO) nanoflakes were covered on the surface of CNTs, simultaneously the interficial carbides Mn_5C_2 were formed during the deposition process. The Mn(MnO)/Mn_5C_2/CNT nanocomposite had electrochemically oxidized conversion from Mn(MnO) to MnO_2 by potential cycling for charge storage, and accordingly made the nanocomposite electrodes with excellent performance, such as

large specific capacitance and excellent cycling stability. These results suggest that such Mn(MnO)/Mn_5C_2/CNTs nanocomposite is very promising for next generation high-performance supercapacitors.

Acknowledgments

The authors gratefully acknowledge the support of the National Natural Science Foundation of China (Nos. 51272226 and 50972125) and the Natural Science Foundation of Hebei Province (No. E2012203112 and E2011203126).

Notes and references

[a] *State Key Laboratory of Metastable Materials Science and Technology, College of Materials Science and Engineering, Yanshan University, Qinhuangdao 066004, PR China. Fax: +86–335–8387679; Tel: +86–13780373375 ; E-mail: diamond_wangyanhui@163.com*

[b] *Tangshan College, Tangshan, hebei 063000, P.R. China*

1.E. Supercapacitors, Kluwer Academic/Plenum, New York, 1999.

2. X. Lu, H. Dou, S. Yang, L. Hao, L. Zhang, L. Shen, F. Zhang and X. Zhang, *Electrochimica Acta*, 2011, 56, 9224-9232.

3. H.-S. Nam, J.-K. Yoon, J. M. Ko and J.-D. Kim, *Materials Chemistry and Physics*, 2010, 123, 331-336.

4. J. R. Miller and P. Simon, *Science Magazine*, 2008, 321, 651-652.

5. J. Wang, J. Polleux, J. Lim and B. Dunn, *The Journal of Physical Chemistry C*, 2007, 111, 14925-14931.

6. J. Yan, E. Khoo, A. Sumboja and P. S. Lee, *Acs Nano*, 2010, 4, 4247-4255.

7. P. Simon and Y. Gogotsi, *Nature materials*, 2008, 7, 845-854.

8. Z. Chen, Y. Qin, D. Weng, Q. Xiao, Y. Peng, X. Wang, H. Li, F. Wei and Y. Lu, *Advanced Functional Materials*, 2009, 19, 3420-3426.

9. F. Teng, S. Santhanagopalan, Y. Wang and D. D. Meng, *Journal of Alloys and Compounds*, 2010, 499, 259-264.

10. V. Subramanian, H. Zhu and B. Wei, *Electrochemistry Communications*, 2006, 8, 827-832.

11. K.-W. Nam, C.-W. Lee, X.-Q. Yang, B. W. Cho, W.-S. Yoon and K.-B. Kim, *Journal of Power Sources*, 2009, 188, 323-331.

12. S.-B. Ma, K.-Y. Ahn, E.-S. Lee, K.-H. Oh and K.-B. Kim, *Carbon*, 2007, 45, 375-382.

13. X. Xie and L. Gao, *Carbon*, 2007, 45, 2365-2373.

14. C.-C. Hu, K.-H. Chang, M.-C. Lin and Y.-T. Wu, *Nano Letters*, 2006, 6, 2690-2695.

15. J.-H. Kim, K. Zhu, Y. Yan, C. L. Perkins and A. J. Frank, *Nano letters*, 2010, 10, 4099-4104.

16. X.-C. Dong, H. Xu, X.-W. Wang, Y.-X. Huang, M. B. Chan-Park, H. Zhang, L.-H. Wang, W. Huang and P. Chen, *ACS nano*, 2012, 6, 3206-3213.

17. G. Yu, L. Hu, N. Liu, H. Wang, M. Vosgueritchian, Y. Yang, Y. Cui and Z. Bao, *Nano Letters*, 2011, 11, 4438-4442.

18. Y. Hou, Y. Cheng, T. Hobson and J. Liu, *Nano letters*, 2010, 10, 2727-2733.

19. Q. Li, Z.-L. Wang, G.-R. Li, R. Guo, L.-X. Ding and Y.-X. Tong, *Nano letters*, 2012, 12, 3803-3807.

20. S. Sivakkumar, J. M. Ko, D. Y. Kim, B. Kim and G. Wallace, *Electrochimica Acta*, 2007, 52, 7377-7385.

21. C. Meng, C. Liu, L. Chen, C. Hu and S. Fan, *Nano letters*, 2010, 10, 4025-4031.

22. J. Liu, J. Essner and J. Li, *Chemistry of Materials*, 2010, 22, 5022-5030.

23. R. Liu, J. Duay and S. B. Lee, *Acs Nano*, 2010, 4, 4299-4307.

24. J.-H. Kim, K. H. Lee, L. J. Overzet and G. S. Lee, *Nano letters*, 2011, 11, 2611-2617.

25. S. W. Lee, J. Kim, S. Chen, P. T. Hammond and Y. Shao-Horn, *Acs Nano*, 2010, 4, 3889-3896.

26. Z.-S. Wu, W. Ren, D.-W. Wang, F. Li, B. Liu and H.-M. Cheng, *ACS nano*, 2010, 4, 5835-5842.

27. L. L. Zhang, X. Zhao, M. D. Stoller, Y. Zhu, H. Ji, S. Murali, Y. Wu, S. Perales, B. Clevenger and R. S. Ruoff, *Nano letters*, 2012, 12, 1806-1812.

28. M.-J. Deng, J.-K. Chang, C.-C. Wang, K.-W. Chen, C.-M. Lin, M.-T. Tang, J.-M. Chen and K.-T. Lu, *Energy & Environmental Science*, 2011, 4, 3942-3946.

29. Y. Zhang, N.W. Franklin, R.J. Chen and H.J. Dai, Chem Phys Lett, 2000, 33, 35–41.

30. B. Djurfors, J. Broughton, M. Brett and D. Ivey, *Acta materialia*, 2005, 53, 957-965.

31. D. Dubal, D. Dhawale, R. Salunkhe and C. Lokhande, *Journal of Electroanalytical Chemistry*, 2010, 647, 60-65.

32. J. Yan, Z. Fan, T. Wei, J. Cheng, B. Shao, K. Wang, L. Song and M. Zhang, *Journal of Power Sources*, 2009, 194, 1202-1207.

33. Y. J. Kang, B. Kim, H. Chung and W. Kim, *Synthetic Metals*, 2010, 160, 2510-2514.

34. J. M. Ko and K. M. Kim, *Materials Chemistry and Physics*, 2009, 114, 837-841.

35. Y. Wang, Z. Shi, Y. Huang, Y. Ma, C. Wang, M. Chen and Y. Chen, *The Journal of Physical Chemistry C*, 2009, 113, 13103-13107.